Received: 25 October 2021 | Revised: 20 March 2022 | Accepted: 20 March 2022

DOI: 10.1002/rcs.2396

ORIGINAL ARTICLE

The International Journal of Medical Robotics and Computer Assisted Surgery

WILEY

Endoscopic image luminance enhancement based on the inverse square law for illuminance and retinex

Longfei Wang[1] | Baibo Wu[1] | Xiang Wang[1] | Qingyi Zhu[2] | Kai Xu[1]

[1]School of Mechanical Engineering, Shanghai Jiao Tong University, Shanghai, China

[2]Department of Urology, The Second Affiliated Hospital of Nanjing Medical University, Nanjing, China

Correspondence
Kai Xu, School of Mechanical Engineering, Shanghai Jiao Tong University, Shanghai, China.
Email: k.xu@sjtu.edu.cn

Funding information
National Natural Science Foundation of China, Grant/Award Number: 51722507; National Key R&D Program of China, Grant/Award Numbers: 2019YFC0118004, 2017YFC0110800, 2019YFC0118003

Abstract

Background: In a single-port robotic system where the 3D endoscope possesses two bending segments, only point light sources can be integrated at the tip due to space limitations. However, point light sources usually provide non-uniform illumination, causing the endoscopic images to appear bright in the centre and dark near the corners.

Methods: Based on the inverse square law for illuminance, an initial luminance weighting is first proposed to increase the image luminance uniformity. Then, a saturation-based model is proposed to finalise the luminance weighting to avoid overexposure and colour discrepancy, while the single-scale retinex (SSR) scheme is employed for noise control.

Results: Via qualitative and quantitative comparisons, the proposed method performs effectively in enhancing the luminance and uniformity of endoscopic images, in terms of both visual perception and objective assessment.

Conclusions: The proposed method can effectively reduce the image degradation caused by point light sources.

KEYWORDS
endoscopic vision, image luminance enhancement, in vivo image enhancement, minimally invasive surgery, point light illumination

1 | INTRODUCTION

1.1 | Motivation

Endoscopic vision plays an important role in robot-assisted minimally invasive surgery (MIS).[1] Based on visual feedback from endoscopes, surgeons can manipulate surgical instruments to perform treatments. In this case, a clear field of view (FOV) is essential to maximise a surgeon's perception and recognition of the surgical scene. However, the visual feedback from endoscopic images is easily affected by endoscopic illumination.

In a single-port robotic system where the 3D endoscope possesses two bending segments as shown in Figure 1A, the remaining space inside the endoscope may only allow point light sources to be used for endoscopic illumination. However, point light sources usually cannot provide uniform illumination. This drawback causes the captured endoscopic images to appear bright in the centre and dark near the corners, as shown in Figure 1B. Additionally, point light illumination produces direct lighting in the centre of the camera view. When a metal gripper appears in the centre, strong light is reflected into the camera lens. As a result, the camera's integrated autoexposure adjustment automatically dims the picture, as shown in Figure 1C.

Unfortunately, the low-level image processing control in the hardware is beyond access. Aiming at improving luminance uniformity and preventing deterioration of the endoscopic images caused by the non-uniform illumination from point light, this paper proposes a luminance enhancement method.

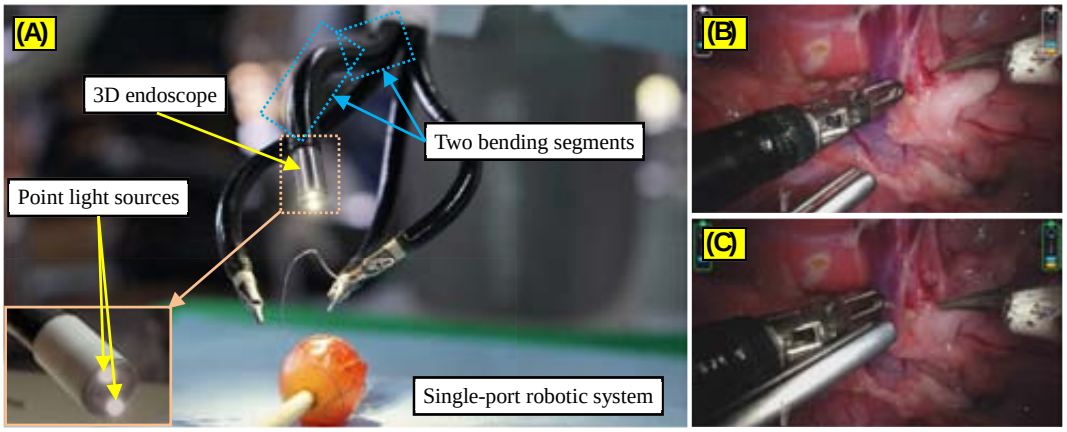

FIGURE 1 (A) The 3D endoscope from a single-port robotic system, (B) endoscopic images that are bright in the centre and dark near the corners, (C) dimmed endoscopic images due to specular reflection

1.2 | Related works

Non-uniform illumination can deteriorate endoscopic images. However, improving illumination uniformity on the device level can hardly handle arbitrary circumstances in an abdominal environment. Hence, a majority of the existing investigations focus on image processing for enhancement.

Luminance-uniformity enhancement is often achieved by reproducing or nonlinearly mapping the pixel's intensity in the image. The surveyed existing methods include (i) retinex-based methods, (ii) dynamic range synthesis or adjustment methods, (iii) frequency domain processing methods, and (iv) neural network methods.

Retinex theory describes the human visual perception of object colour and brightness.[2] It assumes that an image can be separated into illumination and reflectance components. Early retinex-based methods for luminance-uniformity enhancement, such as the single-scale retinex (SSR)[3] and the multiscale retinex (MSR),[4] ignore the non-uniform illumination component and treat the reflectance component as the outcome. However, the reflectance component of SSR often looks unnatural,[5] while the reflectance component of MSR may exhibit streak-like and greyish artefacts when the input image is non-uniformly illuminated. To overcome the drawbacks of MSR, Luo et al.[6] applied a bilateral filter to each level of the MSR model to obtain an artefact-removed reflectance component. Then the dynamic range of the reflectance component is stretched to generate the output with proper contrast and sharpness. However, this method can lead to a bright or overenhanced image if the histogram percentage is inappropriately used. The naturalness preserved enhancement (NPE) method[7] enhances contrast while preserving the naturalness of illumination. However, the computational efficiency can be improved.

In addition to processing the reflectance component, enhancing the illumination component is another adopted method to improve the uniformity of an image. For example, Okuhata et al.[8] applied a gamma correction (GC) for the estimated illumination to nonlinearly enhance the luminance of endoscopic images. Xia et al.[9] divided the estimated illumination component in endoscopic images into well-lit, low-light and lossy regions. The well-lit regions were preserved, and the other two regions were gamma-corrected to achieve luminance improvements. However, directly applying GC to image luminance may result in oversaturation. Fu et al.[10] proposed a multiscale fusion (MF) method that fuses luminance-enhanced illumination components and contrast-enhanced illumination components to improve image luminance while preserving contrast. Then, the same authors[11] later proposed an optimisation strategy that changes the penalty in the variational retinex framework, to more accurately complete simultaneous reflection and illumination estimation (SRIE). The estimated illumination component is then enhanced by GC. Similarly, Guo et al.[12] optimised the illumination estimation method and achieved low-light image enhancement (LIME) via gamma correcting the illumination component. However, these methods might be less suitable when handling a surgical scene, as shown in the experiments.

In addition, the high-dynamic range (HDR) method synthesises an endoscopic outcome with more than one same-scene image with different exposures, leading to a reduced video frame rate. Histogram equalisation (HE)-based methods[13,14] can stretch the dynamic range of image luminance to augment details. However, the HE-based method enhances the contrast in an endoscopic image rather than adjusting the luminance, possibly generating overenhanced or underenhanced results.[15]

In terms of frequency-domain processing methods for image quality enhancement, Sdiri et al.[16] used joint wavelet decomposition with adjusted subband coefficients to enhance the image's luminance and details. However, the transformation from the spatial domain to the frequency-domain is time-consuming.

The neural network methods can also be used to improve endoscopic image luminance, for example, a modified U-Net architecture[17] was trained with low-light images to enhance laryngeal images. However, sufficient training images can be rarely obtained for a much more complex abdominal environment, particularly during surgical treatments.

Other related image enhancement works, including the use of i-scan technology,[18] sigmoid function,[19] disparity information,[20] tri-scan technology,[21] and texture and colour information,[22] primarily enhance image contrast, instead of luminance uniformity.

The colour correction methods, including the look-up table method,[23] chromaticity correction,[24] polynomial colour correction (PCC),[25] root-polynomial colour correction (RPCC),[26] and dynamic colour correction matrix,[27] only improve the colour presentation, unlike the proposed method, which enhances luminance uniformity and preserves colour correctness.

The endoscope views in[21,22] all have their four corners cut, mostly because of the lower luminance at the corners. It is clear that the proposed algorithm is in great need of improving the uniformity of image luminance, while preserving the correct colour and maintaining the noise level to enhance the viewable area of endoscopes.

1.3 | Contributions

Inspired by the illuminating property of point light sources,[28,29] an initial luminance weighting is first proposed to increase the uniformity of image luminance, based on the inverse square law of illuminance. Since the increased image luminance may cause colour discrepancies and overexposure, a saturation-based method for luminance weighting is then proposed to reduce the colour discrepancy and overexposure. Furthermore, improving the luminance of a low-light image may cause an enhanced noise level. However, directly applying a low-pass filter loses the image's high-frequency information and reduces its sharpness. A separation between the reflectance component and the illumination component of image luminance is hence obtained based on the SSR scheme. Then, only applying a guided filter for the reflectance component reduces the noise in the high-frequency-domain but retains the preferred details.

This paper's main contributions are summarised as follows.

1. Based on the inverse square law and considering the geometry between the cameras and the light sources, an initial luminance weighting is proposed to assign different enhancement weights for different pixels. Thus, different levels of enhancement in pixel luminance of the endoscopic images are achieved.
2. To avoid overexposure and colour discrepancy after enhancing the image luminance, this paper proposes a saturation-based approach to finalise the luminance weighting. The saturation model is designed to adaptively assign high enhancement weights to less-saturated pixels and low enhancement weights to highly saturated pixels.
3. To control the noise level while retaining the preferred image sharpness, a guided filter is employed to reduce the noise in the image's reflectance component separated based on the SSR approach.

The effectiveness is verified upon endoscopic images captured from an artificial abdominal cavity and an in vivo porcine model scene, while compared with a few existing state-of-the-art methods. Moreover, the proposed method is also applied to open-access datasets to further verify the effectiveness.

2 | METHODS

The initial luminance weighting based on the inverse square law for illuminance is proposed in Section 2.1. Then, a saturation model for finalising the luminance weighting and the determination of luminance enhancement parameters are presented in Sections 2.2 and 2.3, respectively. A retinex-based model for noise control is presented in Section 2.4. Finally, the implementation flowchart is introduced in Section 2.5.

2.1 | Initial luminance weighting

The stereo endoscopic cameras and the two light sources are arranged for integration compactness, as shown in Figure 2. The distances between the two cameras and two light sources are indicated by d_c and d_s, respectively. The u-axis denotes the direction from the left camera to the right camera with the v-axis denoting the direction from the top light source to the bottom light source.

Illuminance variations associated with a point light source p_{st} can be characterised by the inverse square law as in Equation (1) for the illuminance E_0 at a point p in a known plane.[28,29]

$$E_0(u,v,d,Q_s) = Q_s \cdot \frac{\mathbf{n}^{\mathrm{T}} \cdot \overrightarrow{p_{st}p}}{l(u,v,d)^2 \left|\overrightarrow{p_{st}p}\right|} \tag{1}$$

where d denotes the distance between p_0 and p_{st}, p_0 is the intersection of the camera optical axis and the plane, (u, v, d) denotes the coordinate of point p, $l(u, v, d)$ denotes the distance between p and p_{st}, Q_s denotes the luminous intensity from the light source p_{st}, and $\mathbf{n}$ denotes the normal $\overrightarrow{p_{st}p_0}/|\overrightarrow{p_{st}p_0}|$ of the plane, referring to Figure 2.

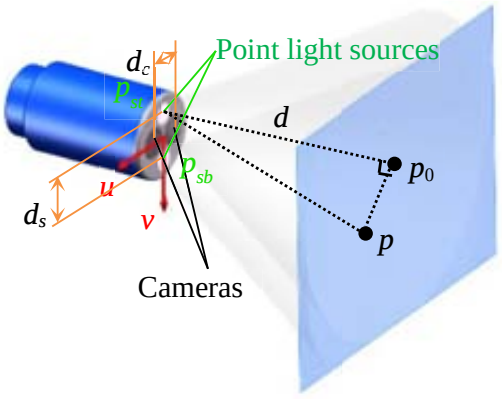

FIGURE 2 Schematic of point light illumination and the arrangement of 3D endoscopic cameras and point light sources

Here, an implication is that the known plane is perpendicular to the camera's optical axis. Compensation for the tilting of this plane is introduced in Section 2.2.

To facilitate the expression of the pixel luminance of the endoscopic image in terms of the illuminance produced by the two point light sources, the coordinate (u, v) is designated at the pixel scale and the conversion scale of pixels per millimetre is expressed as in Equation (2) for the known plane located d mm away.

$$d_{\text{pixel}} = \frac{\sqrt{w_I{}^2 + h_I{}^2}}{2d\tan(\theta_{\text{fov}}/2)} \tag{2}$$

where θ_{fov} is the FOV angle of the camera, and w_I and h_I are the horizontal and vertical resolutions of the captured image, respectively.

Thus, $I^2(u, v, d)$ can be given by $d^2 + ((u - u_0)^2 + (v - v_0)^2)/d_{\text{pixel}}{}^2$, where (u_0, v_0) denotes the $\{uv\}$ coordinate of p_0. The pixel coordinates of the top light source p_{st} and the bottom light source p_{sb} with respect to frame $\{uv\}$ can be obtained as $(0, -d_s \cdot d_{\text{pixel}}/2, 0)$ and $(0, d_s \cdot d_{\text{pixel}}/2, 0)$, respectively.

Under the illumination of p_{st} and p_{sb}, the illuminance of each point on the known plane located d mm away can then be obtained, with respect to the frame $\{uv\}$ shown in Figure 2, as follows:

$$E(u, v, d, Q_s) = E_{st}(u, v, d, Q_{st}) + E_{sb}(u, v, d, Q_{sb}) \tag{3}$$

where $E_{st}(u, v, d, Q_{st})$ and $E_{sb}(u, v, d, Q_{sb})$, corresponding to the illuminance from p_{st} and p_{sb}, are given as follows.

$$\begin{cases} E_{st}(u, v, d, Q_{st}) = \left(Q_{st} \cdot \mathbf{n}^{\mathrm{T}} \cdot \overrightarrow{p_{st}p} \Big/ \left|\overrightarrow{p_{st}p}\right|\right) \Big/ \left(d^2 + \left(u^2 + (v + d_s \cdot d_{\text{pixel}}/2)^2\right) \Big/ d_{\text{pixel}}{}^2\right) \\ E_{sb}(u, v, d, Q_{sb}) = \left(Q_{sb} \cdot \mathbf{n}^{\mathrm{T}} \cdot \overrightarrow{p_{sb}p} \Big/ \left|\overrightarrow{p_{sb}p}\right|\right) \Big/ \left(d^2 + \left(u^2 + \left(v - d_s \cdot d_{\text{pixel}} \Big/ 2^2\right) \Big/ d_{\text{pixel}}{}^2\right)\right) \end{cases} \tag{4}$$

In this paper, Q_{st} equals to Q_{sb} is assumed.

Then, for an image that has a size in $w_I \times h_I$ in pixels and centres on the camera optical axis, the pixel coordinate range with respect to the frame $\{uv\}$ can be represented as $\{(u, v)\ |u_0 - w_I/2 \le u \le u_0 - w_I/2, v_0 - h_I/2 \le v \le v_0 - h_I/2\}$. Here, (u_0, v_0) for the left and right cameras can be given by $(-d_c d_{\text{pixel}}/2, 0)$ and $(d_c d_{\text{pixel}}/2, 0)$, respectively. Thus, the illuminance, $E^l(u, v, d, Q_s)$ and $E^r(u, v, d, Q_s)$, corresponding to the left and right endoscopic imaging plane can be obtained from Equation (3) as follows:

$$\begin{cases} E^l = E(u, v, d, Q_s), \text{ when } \left|u + d_c \cdot d_{\text{pixel}}/2\right| \le w_I \Big/ 2, |v| \le h_I \Big/ 2 \\ E^r = E(u, v, d, Q_s), \text{ when } \left|u - d_c \cdot d_{\text{pixel}}/2\right| \le w_I/2, |v| \le h_I/2 \end{cases} \tag{5}$$

The distance d is set to 60 mm in this paper. An explanation for using 60 mm is provided in Section 3.2.

An *illuminance map* $M(u, v)$ is formulated as in Equation (6) to facilitate the initial luminance weighting calculation. In this way, Q_s is eliminated from $M(u, v)$ and a weight of one is assigned to the pixel with the highest illuminance, while increased weight values are assigned to the pixel with lower illuminance. $M(u, v) \ge 1$ is constant for a specific distance d. $M(u, v)$ does not have a superscript for brevity, because the handling of the left and the right images is similar.

$$M(u, v) = E^{l/r}_{\max} \Big/ E^{l/r}(u, v, d, Q_s) \tag{6}$$

The initial luminance weighting $W_1(u, v)$ is defined as in Equation (7).

$$W_1(u, v) = k_1 \cdot (M(u, v) - 1) \tag{7}$$

where k_1 is a coefficient obtained from the image luminance as explained in Section 2.3, and mainly influences the luminance of the image corner region.

2.2 | Smoothed saturation-based luminance weighting

Directly applying the initial luminance weighting may oversaturate an image's near-saturated pixels and over-increase the luminance of pixels, leading to colour discrepancy and overexposure. Hence, a saturation-based model is proposed to finalise the luminance weighting.

First, 2D gamma correction (2D-GC) as in Equation (8) is introduced to generate enhancement weights for each pixel. This applied 2D-GC is modified from[30] by determining the saturation-related factor α based on the image saturation component and adjusting a reference value s_{ref} for endoscopic images. The saturation of a pixel is denoted as $S(u, v) \in [0,1]$.

$$g(S(u, v), s_{\text{ref}}, \alpha) = S(u, v)^{\gamma}, \ \gamma = \alpha^{\left(\frac{s_{\text{ref}} - S(u,v)}{s_{\text{ref}}}\right)}, \ s.t.\{0 < \alpha \le 1, 0 < s_{\text{ref}} < 1\} \tag{8}$$

where $g(\cdot)$ denotes the 2D-GC function. The s_{ref} can partition low and high saturation values, while α can yield different changes in the results of the 2D-GC. The influences of α and s_{ref} on the saturation value are shown in Figure 3. The determination of α and s_{ref} is explained in Section 2.3.

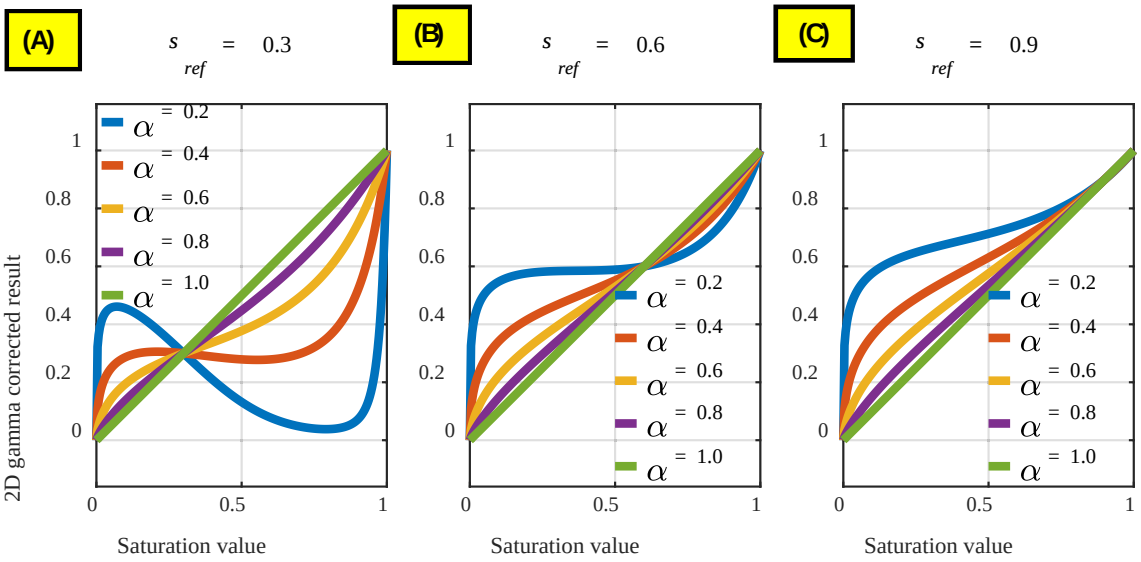

FIGURE 3 Effects of the modified 2D gamma correction, where s_{ref} is set to 0.3, 0.6, and 0.9 in (A–C), respectively

Please note that nonlinear correction above can also compensate for possible tilting of the known plane that is modelled in Section 2.1. When the known plane is tilted, the point closer to the light source will have higher luminance and higher saturation will appear in the corresponding pixel. In contrast, the pixel corresponding to the point farther from the light source will have lower luminance and lower saturation.

The luminance weighting adjusted by the nonsmooth saturation component may increase the local noise of the image. Hence, a mean filter $F_{mean}(u, v, r_m)$ is applied in the saturation $S(u, v)$ before the 2D-GC. Then, Equation (8) is modified as follows:

$$g(O_{mean}(u,v), s_{ref}, \alpha) = (O_{mean}(u,v))^{\gamma},$$
$$\gamma = \alpha^{\left(\frac{s_{ref} - O_{mean}(u,v)}{s_{ref}}\right)}, \quad O_{mean}(u,v) = F_{mean}(u,v,r_m) \otimes S(u,v) \tag{9}$$

where $\otimes$ denotes the convolution operator, $O_{mean}(u, v)$ denotes the smoothed saturation component output, and r_m denotes the radius of the kernel of the mean filter. r_m is experimentally set to 7 which is the smallest radius value that can produce the enhanced image with less noticeable noise in this paper.

Finally, the luminance weighting for the luminance component is finalised as follows.

$$W_2(u,v) = (W_1(u,v) + k_2) \cdot g(O_{mean}(u,v), s_{ref}, \alpha) + 1 \tag{10}$$

where a constant, 1, is added at the right side of Equation (10) to avoid zero value assigned to $W_2(u, v)$, k_2 is a coefficient designed to further improve or decrease the average luminance of an endoscopic image. The value of k_2 is obtained from the image luminance as explained in Section 2.3.

2.3 | Enhancement parameter determination

To adaptively determine k_1, the uniformity U of an endoscopic image is defined as in Equation (11).

$$U = L_{corner}/L_{center} \tag{11}$$

where L_{center} and L_{corner} denote the average luminance in the centre ROI (region of interest) and the corner ROIs of an image, respectively, referring to Figure 4.

For ideal uniformity, U equals to 1. Thus, k_1 is set as in Equation (12).

$$k_1 = 1/U \tag{12}$$

The average value L_m of luminance of an endoscopic image is used to determine k_2, as in Equation (13).

$$k_2 = \log_2\left(L_m^{ref} - L_m + 1\right) \tag{13}$$

where the logarithm function is deployed to adjust the enhancement magnitude of image luminance referring to the sensitivity of the human visual system,[3] and L_m^{ref} denotes the reference value obtained from the histogram of L_{center} of 68 820 endoscopic images from the video sequences recorded during a few endoscopic MISs, as shown in Figure 5A. The Gaussian-fitted mean value of the histogram reflects the most common L_{center} value; thus, L_m^{ref} is set to 0.5207.

According to Section 2.2, a smaller α can yield a larger change in the results of the 2D-GC. Thus, α is set as the average image saturation S_m as in Equation (14), since S_m and L_m are proportional (as shown in Figure 5B), and larger weights should be assigned to the dimmer endoscopic images.

$$\alpha = S_m = \frac{1}{h_I w_I} \sum_{v=1}^{h_I} \sum_{u=1}^{w_I} S(u,v) \tag{14}$$

Based on k_1, k_2, and α, the involved endoscopic images are enhanced with different s_{ref}, as shown in Figure 6. The brightness of the images decreases from Figure 6B–F. Figure 6D–F shows acceptable colour according to the surgeon author. Considering the 2D-GC is modified to reduce the enhancement weights of high saturation pixels, s_{ref} is suggested to be set to 0.6 by the surgeon author in this paper.

2.4 | SSR-based noise control

Directly increasing the luminance of an image may result in an increased noise level. An intuitive method to reduce the noise associated with the luminance level is by filtering the luminance component of an image. However, the filtered luminance intensity will likely exclude high-frequency details.

Thus, the SSR method as in Equation (15) is used to separate the reflectance component $R(u, v)$ containing image high-frequency information.

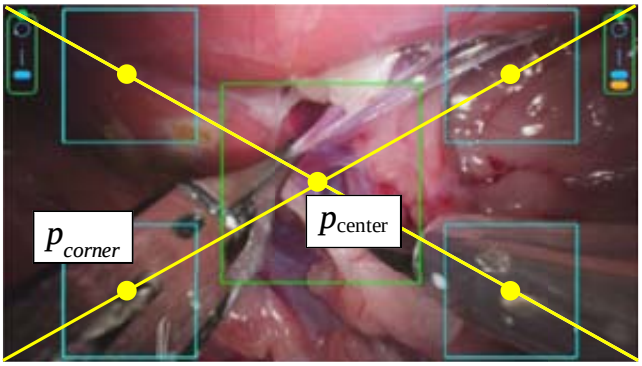

FIGURE 4 Region of interests (ROIs) for image uniformity calculation. The green square denotes the centre ROI (601 pixel × 601 pixel), while the cyan squares denote the corner ROIs (401 pixel × 401 pixel). The yellow points denote the centre of each ROI

$$\begin{aligned}\log(R(u,v)) &= \log(L(u,v)) - \log\left(O_{\text{gaussian}}(u,v)\right), \quad O_{\text{gaussian}}(u,v) \\ &= F_{\text{gaussian}}\left(u,v,r_{gu},\sigma\right) \otimes L(u,v)\end{aligned} \tag{15}$$

where $L(u, v)$ denotes the luminance of a pixel, and $F_{\text{gaussian}}(u, v, r_{gu}, \sigma)$ and $O_{\text{gaussian}}(u, v)$ denote the Gaussian filter and the smoothed luminance output, respectively. The Gaussian kernel radius r_{gu} is empirically set to 3, and the Gaussian variance σ is experimentally set to 5.

Then, the fast guided filter[31] is applied to $R(u, v)$ as in Equation (16), for denoising while retaining the preferred high-frequency details.

$$O_{\text{guided}}(u,v) = F_{\text{guided}}\left(u,v,r_{ga},\varepsilon,s\right) \otimes R(u,v) \tag{16}$$

where $F_{\text{guided}}(u, v, r_{ga}, \varepsilon, s)$ and $O_{\text{guided}}(u, v)$ denote the fast guided filter and the noise-reduced reflectance component output, r_{ga}, ε, and s denote the radius, regularisation parameters, and subsampling ratio of the fast guided filter.[31] r_{ga} and s are set to 16 and 4, respectively, according to He's work,[31] and ε is experimentally set to 0.0035.

Finally, the inverse SSR approach is applied based on $O_{\text{guided}}(u, v)$ to produce noise-reduced image luminance $L'(u, v)$, as in Equation (17).

$$\log\left(L'(u,v)\right) = \log\left(O_{\text{guided}}(u,v)\right) + \log\left(O_{\text{gaussian}}(u,v)\right) \tag{17}$$

2.5 | Implementation

A flowchart of the proposed method for implementing endoscopic image luminance enhancement is summarised in Figure 7. The illuminance map $M(u, v)$ is precalculated once the parameters of an endoscope are known, as summarised in the blue dotted region in Figure 7. The input image is converted into the HSV space. Then, the two enhancement parameters, k_1 and k_2, are obtained using Equations (12) and (13). Next, the S component is used to finalise the

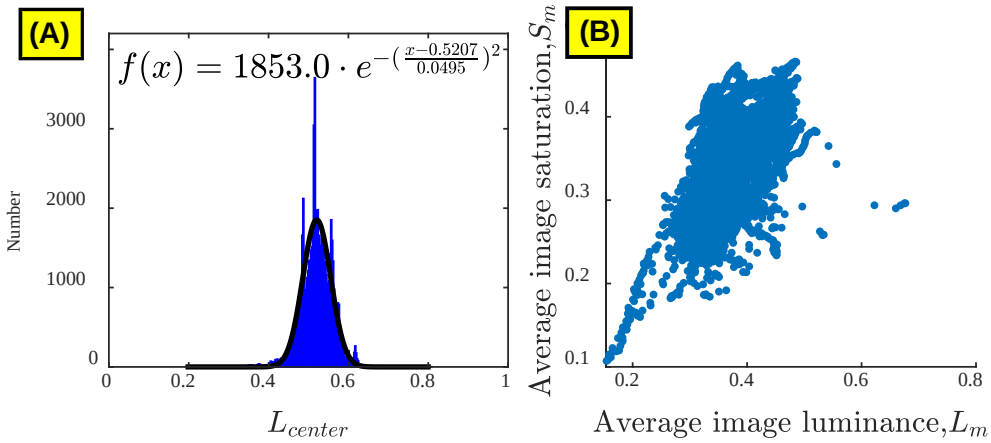

FIGURE 5 (A) Histogram of L_{center} of the 68 820 endoscopic images and (B) the scatter plot between average image luminance L_m and average image saturation S_m of the 68 820 endoscopic images

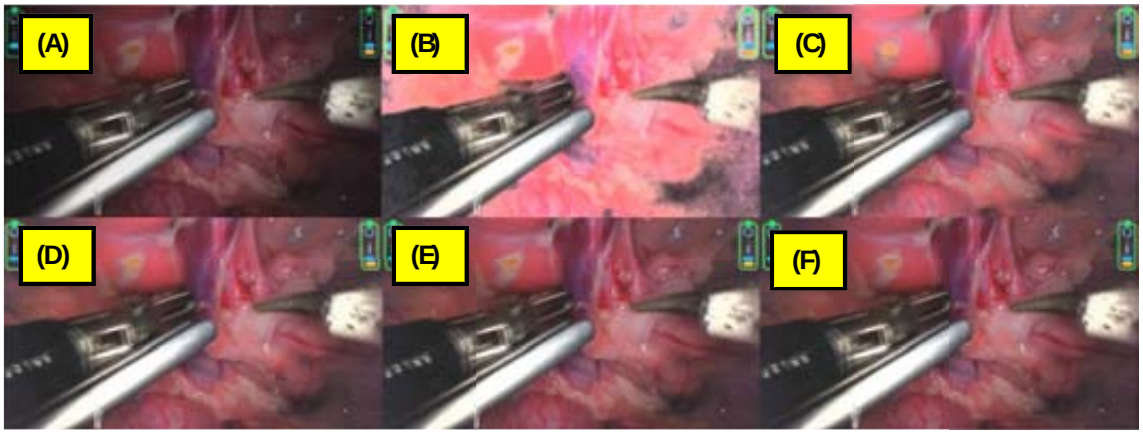

FIGURE 6 Luminance enhancement with different s_{ref}: (A) original endoscopic image, (B–F) the enhanced results with s_{ref} set to 0.2, 0.4, 0.6, 0.8, and 1.0, respectively

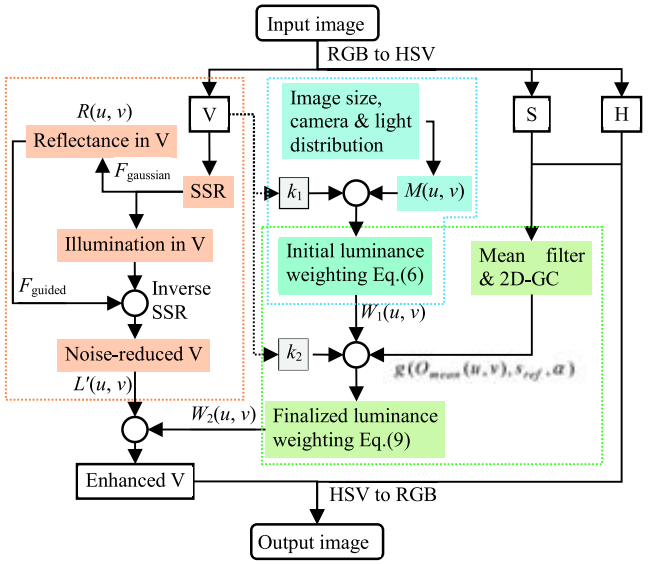

FIGURE 7 Flowchart of the luminance enhancement scheme for endoscopic images

luminance weighting, as summarised in the green dotted region in Figure 7. After obtaining the noise-reduced V component based on the SSR approach (as summarised in the orange dotted region in Figure 7), the enhanced image luminance is obtained through elementwise multiplication with luminance weighting. Finally, the output image is reproduced by converting the enhanced *V* component, the original *H*, and the original *S* components into the RGB colour space.

3 | EXPERIMENTAL SETTINGS

This section first introduces the utilised image quality assessment methods. Then, the luminance maps for the deployed stereo endoscopic image are obtained based on the geometry between the endoscopic cameras and the light sources.

3.1 | Image quality assessment

In general, objective image quality assessment (IQA) methods can be categorised into full-reference IQA, reduced-reference IQA, and no-reference IQA methods.[32] The first IQA method requires full information from a reference image. However, it is difficult to obtain such endoscopic images with full ground truth as the reference images.

Hence, experimental verifications are conducted, using (i) reduced-reference IQA methods, (ii) no-reference IQA methods, and (iii) open-access dataset images.

For reduced-reference IQA, images containing an X-Rite ColorChecker Classic Mini chart that is referred to as ColorChecker and shown in the inset in Figure 9A are captured inside an artificial abdominal model. Two reduced-reference IQA metrics, including the mean colour difference (mean ΔE) metric and the signal-to-noise ratio (SNR) metric, are assessed on these images referring to the ColorChecker region before and after the enhancement. The mean ΔE is evaluated in CIELAB colour space[33] based on the ColorChecker. The SNR is calculated as the average SNR based on the white-grey-black patches in the ColorChecker region.

For no-reference IQA, the image quality of the in vivo images obtained from the video sequences recorded during a few endoscopic MISs is assessed before and after the enhancement. Additionally, our method is compared with several state-of-the-art methods. Because no ColorChecker is used in such a setting, four no-reference IQA metrics, including contrast, colourfulness, luminance-uniformity, and a proposed hybrid metric, are used to assess the quality of the images. A brief description of the adopted no-reference IQA is as follows.

3.1.1 | Contrast metric

Image contrast is evaluated by the root mean square, and is calculated as in Equation (18).

$$Contrast = \sqrt{\frac{1}{h_l w_l}\sum_{i=1}^{h_l}\sum_{j=1}^{w_l}\left(L_{i,j} - L_m\right)^2} \tag{18}$$

where L_m is defined in Equation (13).

3.1.2 | Colourfulness metric

Colourfulness is the attribute of chrominance information humans perceive. The evaluation of colourfulness is given by Equation (19), according to an existing study.[34]

$$Colorfulness = 0.02 \cdot \log\left(\frac{\sigma_\alpha^2}{|\mu_\alpha|^{0.2}}\right) \cdot \log\left(\frac{\sigma_\beta^2}{|\mu_\beta|^{0.2}}\right) \tag{19}$$

where $\alpha = R - G$, $\beta = 0.5(R + G) - B$, and σ_α^2, σ_β^2, μ_α, μ_β represent the variance and mean values of α and β.

3.1.3 | Luminance-uniformity metric

The proposed method can improve the uniformity and enhance the luminance of the endoscopic images, so the luminance-uniformity metric is defined as a weighted summation of uniformity and average luminance of an image in this paper, as given in Equation (20).

$$Luminance\_Uniformity = 0.5 \cdot \left(1 - \left|L_m - {L_m}^{\text{ref}}\right|\right) + 0.5 \cdot U,\ Luminance\_Uniformity \in [0, 1] \tag{20}$$

where L_m, ${L_m}^{\text{ref}}$, and U are defined in Equations (13) and (11).

3.1.4 | Hybrid metric

Image contrast may be reduced when the global luminance range is compressed to enhance dark regions in an image,[10] so a larger *Contrast* value denotes better results after the image luminance is improved. Accordingly, a hybrid metric named the *CCLU* metric is proposed as given in Equation (21). The reason for using multiplication is that the contrast, the colourfulness, and the luminance-uniformity metrics are on different scales.

$$CCLU = Contrast \cdot Colorfulness \cdot Luminance\_Uniformity \tag{21}$$

Moreover, to further verify the effectiveness of the proposed method, the images obtained from the Hamlyn Centre Laparoscopic/Endoscopic Video Datasets are used to show the robustness of the proposed method, because the lighting conditions were unknown.

3.2 | Obtaining the illuminance maps

A stereo HD endoscope with a resolution of 1920 × 1080 is used to verify the proposed method.

The distance d_c between the two endoscopic cameras is 4.05 mm, and the distance d_s between the two point light sources is 7.00 mm. The θ_{fov} of the endoscopic camera is 90°. The working distance of the endoscope ranges from 30 to 120 mm, and the range from 50 to 70 mm is a comfortable viewing distance. The comfortable viewing distance is recommended by the surgeon author. To determine a suitable working distance for creating the illuminance map $M(u, v)$, the maximum value of $M(u, v)$, that is, $E_{\text{max}}/E_{\text{min}}$, at different working distances is first calculated, as listed in Table 1. Since the variation in $E_{\text{max}}/E_{\text{min}}$ is small for the deployed endoscope, considering the comfortable working distance of the endoscope, the distance for calculating the luminance map is set to 60 mm.

The illuminance map $M(u, v)$ is obtained by substituting the parameters above into Equations (2)–(6). Figure 8 shows the normalised $M(u, v)$ obtained for the stereo endoscopic cameras.

4 | EXPERIMENTS AND RESULTS

The animal studies involved in this section were approved by the Shanghai Yinshe Clinical Centre, Shanghai, China, which is a qualified company to issue ethics certification and offer sites for animal studies.

4.1 | Reduced-reference IQA: enhancement on ColorChecker images

The setup for capturing the endoscopic images containing a ColorChecker is shown in Figure 9. A cold light source and an optical fibre

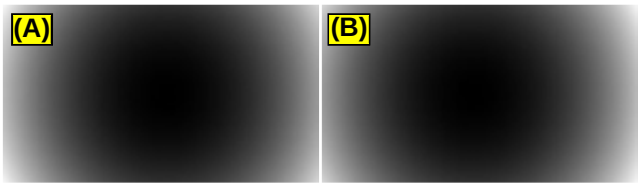

FIGURE 8 Illuminance maps for the endoscopic cameras at a working distance of 60 mm for the (A) left camera and (B) right camera

TABLE 1 Maximum value of the illuminance map at 60 mm working distance

Wording distance (mm)	30	40	50	60	70	80	90	100	110	120
$E_{\text{max}}/E_{\text{min}}$	3.0829	3.0150	2.9755	2.9489	2.9295	2.9155	2.9051	2.8965	2.8896	2.8844

cord provide endoscopic illumination, as shown in Figure 9A. While capturing the ColorChecker images, an artificial abdominal model was covered, as shown in Figure 9B,C to mimic the abdominal cavity. The intensity of the light source was manually adjusted to create an environment with different illuminance levels. The scene in the abdominal model was viewed on a laptop, as in Figure 9A,C.

The captured ColorChecker images are shown in the first row of Figure 10. All of these images appear bright in the centre and dark around the corners. A ColorChecker was placed in different locations to assess the improvement in image quality in different regions. A low-light image as in Figure 10C was included for further verification.

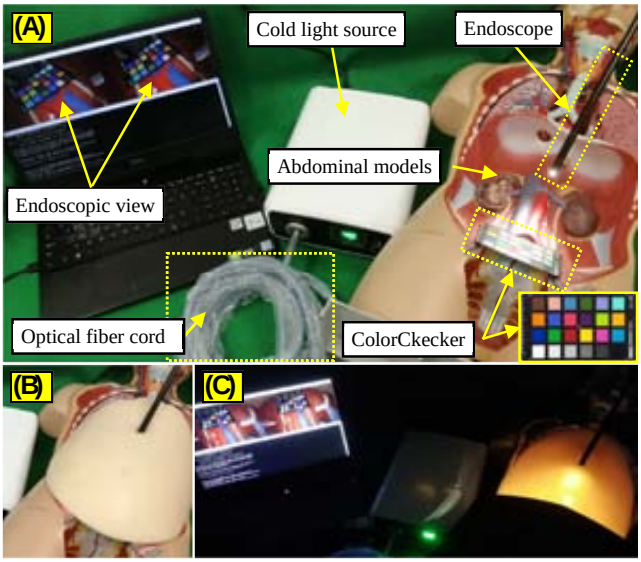

FIGURE 9 Setup for capturing endoscopic images containing a ColorChecker: (A) the hardware used to capture images, (B) the covered artificial abdominal cavity, and (C) the scene during image captures

The corresponding enhanced results are shown in the second row of Figure 10. Enhanced visibility can be perceived from these enhanced images. The reduced-reference IQA metric values and the enhancement parameters k_1 and k_2 for these images are listed in Table 2 k_1 and k_2 are obtained according to Equations (11) and (12), respectively.

Table 2 shows that the colour accuracy in the well-lit region slightly deteriorates, referring to the first row, but the colour difference in the low-light region is reduced referring to the second to third rows of Table 2.

For the colour accuracy in Figure 10A, the ColorChecker is placed in the centre of the endoscopic image with good lighting conditions. In this case, an accurate and near-saturated colour is produced. Then, if the luminance of the pixel is further improved, the colour of the pixel tends to be oversaturated, thereby reducing the accuracy of the pixel colour. Due to the illumination nature from the point light source, well-lit regions are always limited. Our methods can still benefit the overall image representation.

The SNR was improved for the white-grey-black patch region in all cases, referring to Table 2.

4.2 | No-reference IQA: comparison with the state of the art

This section presents comparisons between the proposed method and several existing state-of-the-art methods, including the adaptive histogram equalisation (AHE) method, the GC method, the NPE method,[7] the MF method,[10] the SRIE method,[11] and the LIME method.[12] The AHE method is achieved by processing the V component in the HSV colour space by the *adapthisteq* function in MATLAB. The GC method is achieved by $V^{0.6}$. The codes of the NPE, MF, SRIE, and LIME methods are also in MATLAB, and are publicly

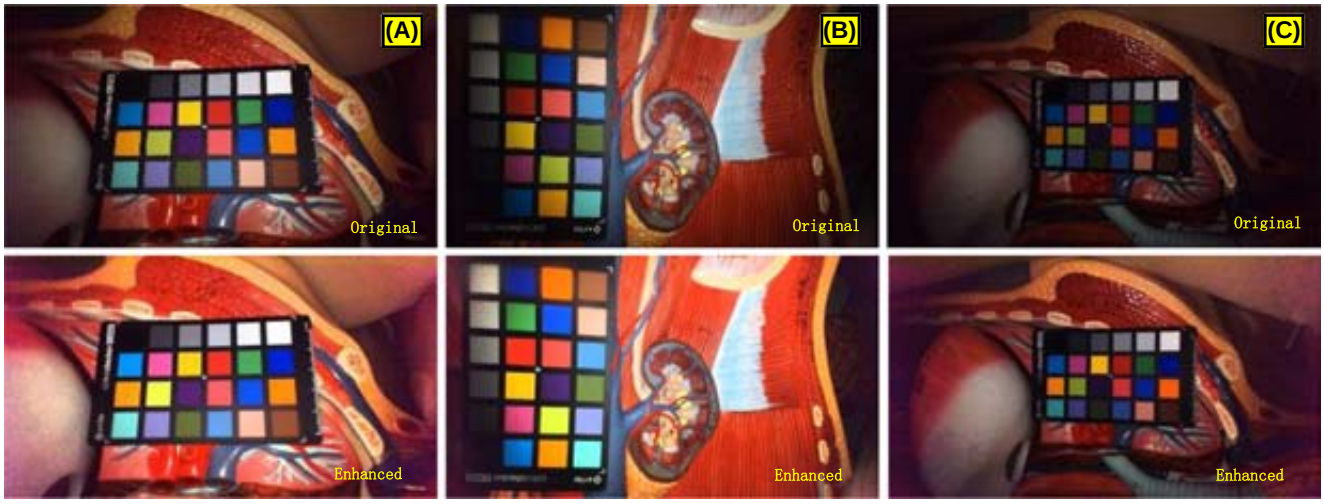

FIGURE 10 Experimental enhancement of the endoscopic images containing the ColorChecker. The first row represents the original images, while the second row represents the corresponding enhanced results

TABLE 2 The enhanced parameters for the ColorChecker images and the assessment results before and after enhancement

	Before enhancement				After enhancement	
Index	Mean ΔE	SNR	k_1	k_2	Mean ΔE	SNR
(a)	8.45	37.5	1.64	0.21	<u>11.02</u>	**43.2**
(d)	19.53	29.1	1.87	0.20	**14.53**	**37.0**
(f)	25.87	35.6	1.44	0.41	**17.08**	**36.3**

Note: **Bold font values** denote that the assessment results for the enhanced images are better than the assessment results for the original images, and <u>underlined values</u> denote the opposite situation.

available from the author's websites. The comparisons are implemented on a laptop with an Intel i7-8750H 2.20 GHz CPU, and 16 GB RAM.

Representative in vivo endoscopic images, as shown in the first row of Figure 11, were obtained from the video sequences recorded during animal studies by the authors' robotic surgical system. Figure 11A–C show three in vivo scene images with common illumination intensity, and Figure 11D,E show two endoscopic images affected by specular reflection. Figure 11E includes an overexposed region, which is used to further verify the effectiveness of the proposed method in avoiding further increasing overexposure.

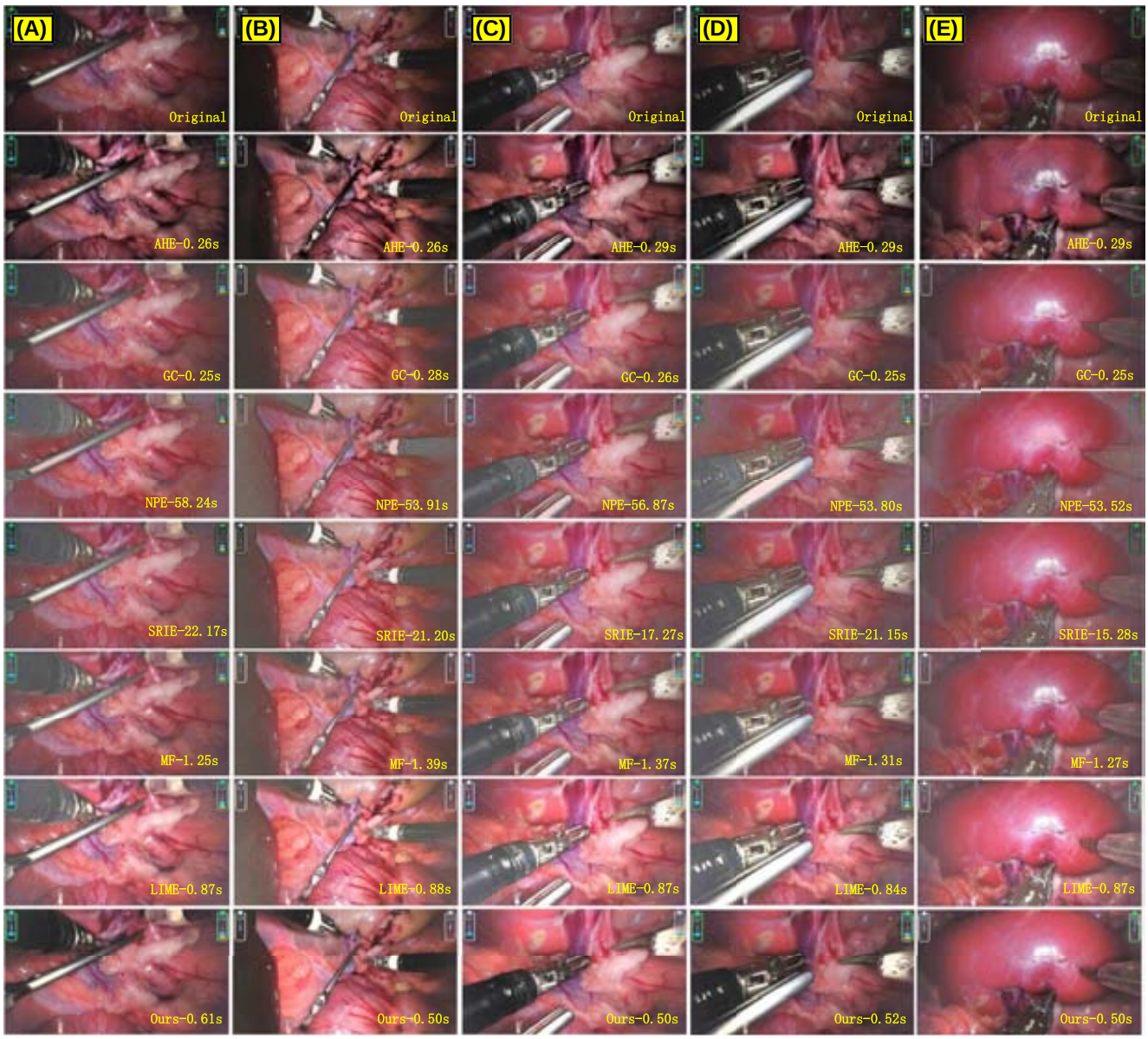

FIGURE 11 Comparison between the proposed method and several state-of-the-art enhancement methods. The first row represents the original in-vivo images. The second to the end rows show the original images enhanced by the AHE, GC, NPE, SRIE, MF, LIME, and Ours methods, respectively. The yellow labels on the enhanced images show the applied methods and the corresponding computational time.

The corresponding enhanced results for the in vivo images and the time consumption are shown in the second to the ninth row of Figure 11. The no-reference IQA metric values for these images are listed in Table 3.

Referring to Table 3, almost all the methods can improve the colourfulness of these endoscopic images. The AHE method improves the luminance and enhances the contrast of the endoscopic images, referring to the second row in Table 3. However, the enhanced images appear colour distorted and the image corners still appear dimmed, referring to the second row of Figure 11. The GC method shows good computational efficiency and effectively improves the image luminance-uniformity, referring to the third row in Figure 11 and Table 3, but the image contrast is reduced compared to the original image.

The NPE, MF, and SRIE methods can effectively improve the luminance-uniformity of the in vivo images, referring to the fourth to sixth rows of Table 3. However, these three methods are time-consuming and also lead to a reduction in image contrast after enhancement. Referring to the seventh row of Figure 11, the enhanced results from the LIME method are close to those from our proposed method, and the LIME performs better in terms of colourfulness referring to the seventh row of Table 3. However, the contrast of the images enhanced by LIME is lower than ours, especially in the black surgical instrument region, referring to the eighth row of Figure 11 and Table 3.

In terms of the overall rating, which is the *CCLU* metric, our proposed method shows the best performance compared to other methods, according to Table 3.

Referring to Figure 11, the enhanced results of GC, NPE, MF, SRIE, and LIME look brighter than ours. However, our method looks more vivid. Since the proposed saturation model can limit the enhancement weight at the pixel level based on image saturation, the neutral colour region, such as the black surgical instrument region in Figure 11A–D, can be preserved. Please note that the black surgical instrument region can increase the intensity difference between the instruments and the tissue textures. The increased intensity difference is beneficial for the human visual system to distinguish the instruments from the in vivo scene, improving the visual quality.[34] Therefore, our method is a well-rounded option.

The overexposure region in the image shown in Figure 11E remains almost unchanged for our method, verifying that a worse overexposure will not be triggered in the proposed saturation-based model.

The proposed method requires approximately 0.53 s to enhance the resolution of 1920 × 1080 endoscopic images in MATLAB 2018a. Therefore, the computational efficiency of our method outperforms the NPE, MF, SRIE, and LIME methods.

4.3 | Image enhancement on open-access datasets

The proposed method was also applied to the Hamlyn Centre Laparoscopic/Endoscopic Video Datasets to further demonstrate the effectiveness.

Several in vivo images from the database are shown in the first row of Figure 12. The first two images were captured in the abdomen in an in vivo porcine procedure and had a resolution of 720 × 288 pixels. The third image shows the cardiac surface and has a resolution of 360 × 288 pixels. The last two images were recorded in an in vivo porcine procedure of diaphragm dissection and had a resolution of 640 × 480 pixels.

Although the geometric parameters, under which the images in the first row of Figure 12 were taken, were unknown, these images were enhanced using the same illuminance map (resized to the sample images) generated by the setting reported in Section 3.2. It is clear that the proposed method still effectively improved the luminance and uniformity of these sample images, referring to the second row of Figure 12.

TABLE 3 Assessment results for the in vivo images before and after enhancement by the proposed and several state-of-the-art methods. All the shown values were multiplied with a factor of 10^1

	Figure 11A				Figure 11B				Figure 11C				Figure 11D				Figure 11F			
Method	C-C-LU metric			*CCLU*	C-C-LU metric			*CCLU*	C-C-LU metric			*CCLU*	C-C-LU metric			*CCLU*	C-C-LU metric			*CCLU*
Original	1.4	5.34	6.79	0.51	1.77	5.72	7.22	0.73	1.71	5.56	7.52	0.71	1.68	5.23	7.22	0.63	1.56	5.46	6.64	0.57
AHE	1.73	5.89	7.65	0.78	1.94	6	8.46	0.98	1.93	5.98	8.14	0.94	1.98	6.08	7.83	0.94	1.67	6.1	7.58	0.77
GC	1.26	6.16	8.32	0.64	1.55	6.21	8.38	0.8	1.5	6.3	8.38	0.79	1.52	6.16	8.64	0.81	1.4	6.28	8.2	0.72
NPE	1.04	6.36	8.46	0.56	1.09	5.7	8.61	0.54	1.21	6.09	8.64	0.64	1.23	6.23	8.92	0.69	1.09	6.23	8.38	0.57
SRIE	1.18	6.39	8.44	0.64	1.41	6.33	8.43	0.75	1.38	6.58	8.41	0.77	1.43	6.45	8.81	0.81	1.29	6.54	8.3	0.7
MF	1.17	6.47	8.52	0.65	1.35	6.22	8.74	0.73	1.36	6.44	8.56	0.75	1.45	6.6	8.8	0.85	1.22	6.58	8.47	0.68
LIME	1.46	7.21	8.06	0.85	1.57	6.97	8.21	0.9	1.62	7.24	8.06	0.95	1.7	7.32	8.4	1.05	1.49	7.34	7.89	0.86
Ours	**1.52**	**6.77**	**8.66**	**0.89**	**1.95**	**7.05**	**8.83**	**1.21**	**1.84**	**7.06**	**8.75**	**1.13**	**1.84**	**6.62**	**9.01**	**1.1**	**1.67**	**7.1**	**8.49**	**1.01**

Note: C-C-LU in this table denotes the contrast, the colourfulness and the luminance-uniformity values. The underlined values denote a few individual metric values that are better than those of ours, even though the overall rating (namely, the *CCLU* value) of our method remains the best.

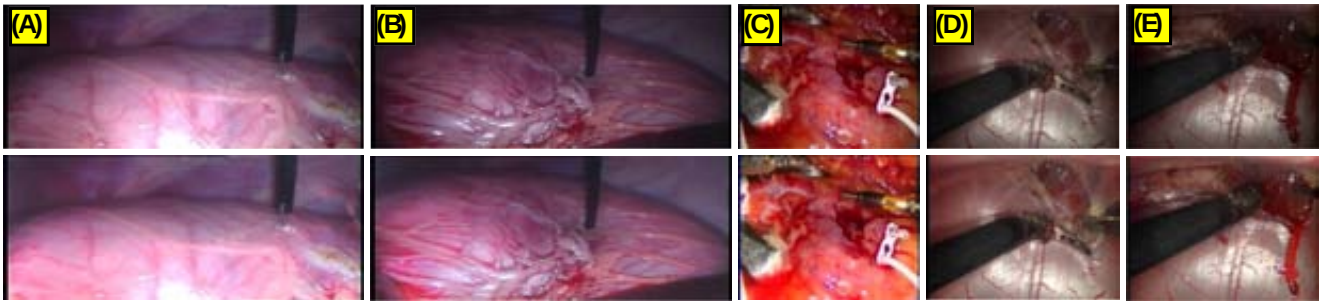

FIGURE 12 Enhancement of a few endoscopic/laparoscopic images from the Hamlyn Centre datasets. The first row shows the original images, while the second row shows the enhanced results by our proposed method

5 | CONCLUSIONS

Since the quality of endoscopic images can be severely affected by unsatisfactory point light illumination, this paper proposes an enhancement method for improving the image luminance and uniformity, while limiting the overexposure, colour discrepancy, and noise level. The proposed method creates an adaptive luminance weighting that can be used to enhance the endoscopic image luminance. The inverse square law for illuminance was first introduced to produce the initial luminance weighting. To avoid overexposure and colour discrepancy after luminance enhancement, a saturation-based model was subsequently introduced, followed by the SSR scheme for noise control.

Experiments were conducted on the scenes from an abdominal model and an in vivo porcine model. To assess the effectiveness of the proposed method, the colour difference, SNR, contrast, colourfulness, and luminance-uniformity were used as the IQA metrics. The experimental results show that the proposed method is effective in improving the colour difference in the low-light region and the SNR in the white-grey-black region. The comparison results show that the proposed method outperforms the AHE methods in improving colourfulness and luminance-uniformity, and outperforms the GC, NPE, MF, SRIE, and LIME methods in terms of the CCLU metric, especially in terms of contrast. Moreover, the proposed method is computationally efficient compared to the NPE, MF, SRIE, and LIME methods. Finally, the experiments on the open-access datasets show that the proposed method is effective for enhancing other endoscopic images.

In the near future, the proposed method is expected to be implemented in an endoscopic surgical system with parallel computing to enable real-time image enhancement.

ACKNOWLEDGEMENTS

This work was supported in part by the National Key R&D Program of China (Grant Nos. 2019YFC0118004, 2017YFC0110800, and 2019YFC0118003), and in part by the National Natural Science Foundation of China (Grant No. 51722507).

CONFLICT OF INTEREST

The authors do not have conflicts of interest in relation to this manuscript.

DATA AVAILABILITY STATEMENT

The source code can be found at: https://github.com/wlfrii/EndoIMLE.

ORCID

Kai Xu https://orcid.org/0000-0003-1690-3370

REFERENCES

1. Taylor RH. A perspective on medical robotics. *Proc IEEE*. 2006;94(9):1652-1664.
2. Land EH. The retinex theory of color vision. *Sci Am*. 1977;237(6):108-129.
3. Jobson DJ, Rahman Z, Woodell GA. Properties and performance of a center/surround retinex. *IEEE Trans Image Process*. 1997;6(3):451-462.
4. Jobson DJ, Rahman Z, Woodell GA. A multiscale retinex for bridging the gap between color images and the human observation of scenes. *IEEE Trans Image Process*. 1997;6(7):965-976.
5. Yue H, Yang J, Sun X, Wu F, Hou C. Contrast enhancement based on intrinsic image decomposition. *IEEE Trans Image Process*. 2017;26(8):3981-3994.
6. Luo X, Zeng H-Q, Wan Y, Zhang X-B, Du Y-P, Peters TM. Endoscopic vision augmentation using multiscale bilateral-weighted retinex for robotic surgery. *IEEE Trans Med Imaging*. 2019;38(12):2863-2874.
7. Wang S, Zheng J, Hu H-M, Li B. Naturalness preserved enhancement algorithm for non-uniform illumination images. *IEEE Trans Image Process*. 2013;22(9):3538-3548.
8. Okuhata H, Nakamura H, Hara S, Tsutsui H, Onoye T. Application of the real-time retinex image enhancement for endoscopic images. In International Conference of the IEEE Engineering in Medicine and Biology Society (EMBC); Osaka, Japan, July 3-7, 2013:3407-3410.
9. Xia W, Chen ECS, Peters T. Endoscopic image enhancement with noise suppression. *Healthc Technol Lett*. 2018;5(5):154-157.
10. Fu X, Zeng D, Huang Y, Liao Y, Ding X, Paisley J. A fusion-based enhancing method for weakly illuminated images. *Signal Process*. 2016;129:82-96.
11. Fu X, Zeng D, Huang Y, Zhang X-P, Ding X. A weighted variational model for simultaneous reflectance and illumination estimation. Paper presented at: IEEE Conference on Computer Vision and Pattern Recognition (CVPR) USA, Las Vegas. 2016:2782-2790.
12. Guo X, Li Y, Ling H. LIME: low-light image enhancement via illumination map estimation. *IEEE Trans Image Process*. 2017;26(2):982-993.
13. Attar A, Xie X, Zhang C, Wang Z, Yue S. Wireless micro-ball endoscopic image enhancement using histogram information. Paper presented at: International Conference of the IEEE Engineering in Medicine and Biology Society (EMBC), Chicago, Illinois, Aug 26–30, 2014;3337-3340.

14. Hai Y, Li L, Gu J. Image enhancement based on contrast limited adaptive histogram equalization for 3D images of stereoscopic endoscopy. Paper presented at: IEEE International Conference on Information and Automation (ICIA), Lijiang, Yunnan, August 8–10, 2015, 2015;668-672.
15. Li M, Liu J, Yang W, Sun X, Guo Z. Structure-revealing low-light image enhancement via robust retinex model. *IEEE Trans Image Process*. 2018;27(6):2828-2841.
16. Sdiri B, Kaaniche M, Cheikh FA, Beghdadi A, Elle OJ. Efficient enhancement of stereo endoscopic images based on joint wavelet decomposition and binocular combination. *IEEE Trans Med Imaging*. 2019;38(1):33-45.
17. Gómez P, Semmler M, Schützenberger A, Bohr C, Döllinger M. Low-light image enhancement of high-speed endoscopic videos using a convolutional neural network. *Med Biol Eng Comput*. 2019;57(7):1451-1463.
18. Kodashima S, Fujishiro M. Novel image-enhanced endoscopy with i-scan technology. *World J Gastroenterol*. 2010;16(9):1043-1049.
19. Imtiaz MS, Wahid KA. Color enhancement in endoscopic images using adaptive sigmoid function and space variant color reproduction. *Computat Math Methods Med*. 2015;2015:1-19.
20. Sdiri B, Beghdadi A, Cheikh FA, Pedersen M, Elle OJ. An adaptive contrast enhancement method for stereo endoscopic images combining binocular just noticeable difference model and depth information. *Electron Imaging*. 2016;2016(13):1-7.
21. Imtiaz MS, Mohammed SK, Deeba F, Wahid KA. Tri-scan: a three stage color enhancement tool for endoscopic images. *J Med Syst*. 2017;41(6):102.
22. Sato T. TXI: texture and color enhancement imaging for endoscopic image enhancement. *J Healthc Eng*. 2021;2021:1-11.
23. Khan TH, Mohammed SK, Imtiaz MS, Wahid KA. Color reproduction and processing algorithm based on real-time mapping for endoscopic images. *SpringerPlus*. 2016;5(1):1–16.
24. Chen J, Wang L-Q, Meng Z-B, Yuan B, Duan H-L. Color correction for high-definition electronic endoscope. *J Innovat Opt Health Sci*. 2012;5(4):1250029.
25. Hong G, Luo MR, Rhodes PA. A study of digital camera colorimetric characterization based on polynomial modeling. *Color Res Appl*. 2001;26(1):76–84.
26. Finlayson GD, Mackiewicz M, Hurlbert A. Color correction using root-polynomial regression. *IEEE Trans Image Process*. 2015;24(5):1460–1470.
27. Wang L, Li Q, Yang H, Huang J, Xu K. A sample-based color correction method for laparoscopic images. Paper presented at: IEEE International Conference on Real-time Computing and Robotics (RCAR); Asahikawa, Japan, 2020.
28. Iwahori Y, Sugie H, Ishii N. Reconstructing shape from shading images under point light source illumination. Paper presented at: International Conference on Pattern Recognition. June, 1990:83-87.
29. Iwahori Y, Iwai K, Woodham RJ, Kawanaka H, Fukui S, Kasugai K. Extending fast marching method under point light source illumination and perspective projection. Paper presented at: International Conference on Pattern Recognition. Aug, 2010:1650-1653.
30. Lee S, Kwon H, Han H, Lee G, Kang B. A space-variant luminance map based color image enhancement. *IEEE Trans Consum Electron*. 2010;56(4):2636-2643.
31. He K, Sun J, Tang X. Guided image filtering. *IEEE Trans Pattern Anal Mach Intell*. 2013;35(6):1397-1409.
32. Kamble V, Bhurchandi KM. No-reference image quality assessment algorithms: a survey. *Optik*. 2015;126(11):1090-1097.
33. Schanda J. Colorimetry: Understanding the CIE System. John Wiley & Sons, Inc.; 2007.
34. Panetta K, Gao C, Agaian S. No reference color image contrast and quality measures. *IEEE Trans Consum Electron*. 2013;59(3):643-651.

How to cite this article: Wang L, Wu B, Wang X, Zhu Q, Xu K. Endoscopic image luminance enhancement based on the inverse square law for illuminance and retinex. *Int J Med Robot*. 2022;e2396. https://doi.org/10.1002/rcs.2396